UNIVERSITY OF CAMBRIDGE

Novel algorithms for the accurate and fast solution of the two-fluid plasma equations

X. Ke Lin, S.T. Millmore, N. Nikiforakis
Laboratory for Scientific Computing, Department of Physics, University of Cambridge
(xk215@cam.ac.uk)

Introduction

Two-fluid plasma model:

- is applicable in a regime between kinetic and MHD models

Background and Motivation

Two-fluid plasma model:

- is applicable in a regime between kinetic and MHD models
- valid in regimes with small length and time scales of the fundamental phenomena, such as those which occur over the Debye length, Larmor radius or plasma frequency scales

Background and Motivation

Two-fluid plasma model:

- is applicable in a regime between kinetic and MHD models
- valid in regimes with small length and time scales of the fundamental phenomena, such as those which occur over the Debye length, Larmor radius or plasma frequency scales
- captures important physical phenomena: charge separation, Lorentz forces, self-generated electromagnetic fields, etc

Background and Motivation

Two-fluid plasma model:

- is applicable in a regime between kinetic and MHD models
- valid in regimes with small length and time scales of the fundamental phenomena, such as those which occur over the Debye length, Larmor radius or plasma frequency scales
- captures important physical phenomena: charge separation, Lorentz forces, self-generated electromagnetic fields, etc
- low-dimensionality compared to the Boltzmann equation

Objectives

- Extending the validity of fluid models in the collisional regime and bridging the gap between fluid and kinetic models

Objectives

- Extending the validity of fluid models in the collisional regime and bridging the gap between fluid and kinetic models
- Reduce computational cost related to small timescales:

Objectives

- Extending the validity of fluid models in the collisional regime and bridging the gap between fluid and kinetic models
- Reduce computational cost related to small timescales:
  - Stiff source terms $\rightarrow$ small CFL number

Objectives

- Extending the validity of fluid models in the collisional regime and bridging the gap between fluid and kinetic models
- Reduce computational cost related to small timescales:
  - Stiff source terms $\rightarrow$ small CFL number
  - **Speed of light constraint** $\rightarrow$ higher than fluid speeds

Objectives

- Extending the validity of fluid models in the collisional regime and bridging the gap between fluid and kinetic models
- Reduce computational cost related to small timescales:
  - Stiff source terms $\rightarrow$ small CFL number
  - **Speed of light constraint** $\rightarrow$ higher than fluid speeds
- Use **divergence-free methods**

Objectives

- Extending the validity of fluid models in the collisional regime and bridging the gap between fluid and kinetic models
- Reduce computational cost related to small timescales:
  - Stiff source terms $\rightarrow$ small CFL number
  - **Speed of light constraint** $\rightarrow$ higher than fluid speeds
- Use **divergence-free methods**
  - Hyperbolic Divergence Cleaning (HDC) is frequently used

Objectives

- Extending the validity of fluid models in the collisional regime and bridging the gap between fluid and kinetic models
- Reduce computational cost related to small timescales:
  - Stiff source terms $\rightarrow$ small CFL number
  - **Speed of light constraint** $\rightarrow$ higher than fluid speeds
- Use **divergence-free methods**
  - Hyperbolic Divergence Cleaning (HDC) is frequently used
    - Divergence errors not completely removed

Objectives

- Extending the validity of fluid models in the collisional regime and bridging the gap between fluid and kinetic models
- Reduce computational cost related to small timescales:
  - Stiff source terms $\rightarrow$ small CFL number
  - **Speed of light constraint** $\rightarrow$ higher than fluid speeds
- Use **divergence-free methods**
  - Hyperbolic Divergence Cleaning (HDC) is frequently used
    - Divergence errors not completely removed
    - There are hyper-parameters

Governing Equations

Governing Equations

The ideal (five-moment) two-fluid plasma equations:

$$\frac{\partial \rho_\alpha}{\partial t} + \nabla \cdot \left(\rho_\alpha \boldsymbol{v}_\alpha\right) = 0 \tag{0.1}$$

$$\frac{\partial \rho_\alpha \boldsymbol{v}_\alpha}{\partial t} + \nabla \cdot \left[\rho_\alpha \boldsymbol{v}_\alpha \otimes \boldsymbol{v}_\alpha + p_\alpha \mathbb{I}\right] = \frac{r_\alpha}{r_{L_i}} \rho_\alpha (\boldsymbol{E} + \boldsymbol{v}_\alpha \times \boldsymbol{B}) \tag{0.2}$$

$$\frac{\partial \mathcal{E}_\alpha}{\partial t} + \nabla \cdot \left[\left(\mathcal{E}_\alpha + p_\alpha\right) \boldsymbol{v}_\alpha\right] = \frac{r_\alpha}{r_{L_i}} \rho_\alpha (\boldsymbol{E} \cdot \boldsymbol{v}_\alpha) \tag{0.3}$$

$$\frac{\partial \boldsymbol{B}}{\partial t} + \nabla \cdot \left(\mathbb{I} \times \boldsymbol{E}\right) = \boldsymbol{0} \tag{0.4}$$

$$\frac{\partial \boldsymbol{E}}{\partial t} + \nabla \cdot \left(-c^2 \mathbb{I} \times \boldsymbol{B}\right) = -\frac{1}{\lambda_D^2 r_{L_i}} (r_i \rho_i \boldsymbol{v}_i + r_e \rho_e \boldsymbol{v}_e) \tag{0.5}$$

where $r_\alpha = q_\alpha / m_\alpha$ and $\alpha = \{\text{ion,electron}\}$

Governing Equations: Fluid Equations

The ideal (five-moment) two-fluid plasma equations:

$$\boxed{\frac{\partial \rho_\alpha}{\partial t} + \nabla \cdot \left(\rho_\alpha \boldsymbol{v}_\alpha\right) = 0}$$

$$\boxed{\frac{\partial \rho_\alpha \boldsymbol{v}_\alpha}{\partial t} + \nabla \cdot \left[\rho_\alpha \boldsymbol{v}_\alpha \otimes \boldsymbol{v}_\alpha + p_\alpha \mathbb{I}\right] = \frac{r_\alpha}{r_{L_i}} \rho_\alpha (\boldsymbol{E} + \boldsymbol{v}_\alpha \times \boldsymbol{B})}$$

$$\boxed{\frac{\partial \mathcal{E}_\alpha}{\partial t} + \nabla \cdot \left[\left(\mathcal{E}_\alpha + p_\alpha\right) \boldsymbol{v}_\alpha\right] = \frac{r_\alpha}{r_{L_i}} \rho_\alpha (\boldsymbol{E} \cdot \boldsymbol{v}_\alpha)}$$

$$\frac{\partial \boldsymbol{B}}{\partial t} + \nabla \cdot \left(\mathbb{I} \times \boldsymbol{E}\right) = \boldsymbol{0}$$

$$\frac{\partial \boldsymbol{E}}{\partial t} + \nabla \cdot \left(-c^2 \mathbb{I} \times \boldsymbol{B}\right) = -\frac{1}{\lambda_D^2 r_{L_i}} \left(r_i \rho_i \boldsymbol{v}_i + r_e \rho_e \boldsymbol{v}_e\right)$$

where $r_\alpha = q_\alpha / m_\alpha$ and $\alpha = \{\text{ion,electron}\}$

Governing Equations: Maxwell Equations

The ideal (five-moment) two-fluid plasma equations:

$$\frac{\partial \rho_\alpha}{\partial t} + \nabla \cdot \left(\rho_\alpha \boldsymbol{v}_\alpha\right) = 0$$

$$\frac{\partial \rho_\alpha \boldsymbol{v}_\alpha}{\partial t} + \nabla \cdot \left[\rho_\alpha \boldsymbol{v}_\alpha \otimes \boldsymbol{v}_\alpha + p_\alpha \mathbb{I}\right] = \frac{r_\alpha}{r_{L_i}} \rho_\alpha (\boldsymbol{E} + \boldsymbol{v}_\alpha \times \boldsymbol{B})$$

$$\frac{\partial \mathcal{E}_\alpha}{\partial t} + \nabla \cdot \left[\left(\mathcal{E}_\alpha + p_\alpha\right) \boldsymbol{v}_\alpha\right] = \frac{r_\alpha}{r_{L_i}} \rho_\alpha (\boldsymbol{E} \cdot \boldsymbol{v}_\alpha)$$

$$\boxed{\frac{\partial \boldsymbol{B}}{\partial t} + \nabla \cdot \left(\mathbb{I} \times \boldsymbol{E}\right) = \boldsymbol{0}}$$

$$\boxed{\frac{\partial \boldsymbol{E}}{\partial t} + \nabla \cdot \left(-c^2 \mathbb{I} \times \boldsymbol{B}\right) = -\frac{1}{\lambda_D^2 r_{L_i}} (r_i \rho_i \boldsymbol{v}_i + r_e \rho_e \boldsymbol{v}_e)}$$

where $r_\alpha = q_\alpha / m_\alpha$ and $\alpha = \{\text{ion,electron}\}$

Governing Equations: Source Terms

The ideal (five-moment) two-fluid plasma equations:

$$\frac{\partial \rho_\alpha}{\partial t} + \nabla \cdot \left(\rho_\alpha \boldsymbol{v}_\alpha\right) = 0$$

$$\frac{\partial \rho_\alpha \boldsymbol{v}_\alpha}{\partial t} + \nabla \cdot \left[\rho_\alpha \boldsymbol{v}_\alpha \otimes \boldsymbol{v}_\alpha + p_\alpha \mathbb{I}\right] = \boxed{\frac{r_\alpha}{r_{L_i}} \rho_\alpha (\boldsymbol{E} + \boldsymbol{v}_\alpha \times \boldsymbol{B})}$$

$$\frac{\partial \mathcal{E}_\alpha}{\partial t} + \nabla \cdot \left[\left(\mathcal{E}_\alpha + p_\alpha\right) \boldsymbol{v}_\alpha\right] = \boxed{\frac{r_\alpha}{r_{L_i}} \rho_\alpha (\boldsymbol{E} \cdot \boldsymbol{v}_\alpha)}$$

$$\frac{\partial \boldsymbol{B}}{\partial t} + \nabla \cdot \left(\mathbb{I} \times \boldsymbol{E}\right) = \boldsymbol{0}$$

$$\frac{\partial \boldsymbol{E}}{\partial t} + \nabla \cdot \left(-c^2 \mathbb{I} \times \boldsymbol{B}\right) = \boxed{-\frac{1}{\lambda_D^2 r_{L_i}} (r_i \rho_i \boldsymbol{v}_i + r_e \rho_e \boldsymbol{v}_e)}$$

where $r_\alpha = q_\alpha / m_\alpha$ and $\alpha = \{\text{ion,electron}\}$

Governing Equations: Divergence Constraints

$$\nabla \cdot \boldsymbol{E} = \frac{\sigma}{\epsilon_0} \tag{0.6}$$

$$\nabla \cdot \boldsymbol{B} = 0 \tag{0.7}$$

where $\sigma = q_i n_i + q_e n_e$ is the net charge density

Numerical Approach

Numerical Approach

- Fluid equations:

Numerical Approach

- Fluid equations:
    - Spatial reconstruction: 2nd-order TVD

Numerical Approach

- Fluid equations:
  - Spatial reconstruction: 2nd-order TVD
  - Hyperbolic solver: HLLC solver

Numerical Approach

- Fluid equations:
  - Spatial reconstruction: 2nd-order TVD
  - Hyperbolic solver: HLLC solver
  - Temporal discretization: explicit RK2

Numerical Approach

- Fluid equations:
  - Spatial reconstruction: 2nd-order TVD
  - Hyperbolic solver: HLLC solver
  - Temporal discretization: explicit RK2
- Maxwell equations $\rightarrow$ divergence-free techniques:

Numerical Approach

- Fluid equations:
  - Spatial reconstruction: 2nd-order TVD
  - Hyperbolic solver: HLLC solver
  - Temporal discretization: explicit RK2
- Maxwell equations $\rightarrow$ divergence-free techniques:
  - **Finite-difference time-domain** (FDTD) [1, 2, 3]

Numerical Approach

- Fluid equations:
  - Spatial reconstruction: 2nd-order TVD
  - Hyperbolic solver: HLLC solver
  - Temporal discretization: explicit RK2
- Maxwell equations → divergence-free techniques:
  - **Finite-difference time-domain** (FDTD) [1, 2, 3]
    - **implicit Crank-Nicolson** [4, 5] → c constraint

Numerical Approach

- Fluid equations:
  - Spatial reconstruction: 2nd-order TVD
  - Hyperbolic solver: HLLC solver
  - Temporal discretization: explicit RK2
- Maxwell equations $\rightarrow$ divergence-free techniques:
  - **Finite-difference time-domain** (FDTD) [1, 2, 3]
    - **implicit Crank-Nicolson** [4, 5] $\rightarrow c$ constraint
  - **Finite-volume time-domain** (FVTD) [6, 7, 8]

Numerical Approach

- Fluid equations:
  - Spatial reconstruction: 2nd-order TVD
  - Hyperbolic solver: HLLC solver
  - Temporal discretization: explicit RK2
- Maxwell equations $\rightarrow$ divergence-free techniques:
  - **Finite-difference time-domain** (FDTD) [1, 2, 3]
    - **implicit Crank-Nicolson** [4, 5] $\rightarrow c$ constraint
  - **Finite-volume time-domain** (FVTD) [6, 7, 8]
    - Spatial reconstruction: 2nd-order TVD or 3rd-order WENO

Numerical Approach

- Fluid equations:
  - Spatial reconstruction: 2nd-order TVD
  - Hyperbolic solver: HLLC solver
  - Temporal discretization: explicit RK2
- Maxwell equations $\rightarrow$ divergence-free techniques:
  - **Finite-difference time-domain** (FDTD) [1, 2, 3]
    - **implicit Crank-Nicolson** [4, 5] $\rightarrow c$ constraint
  - **Finite-volume time-domain** (FVTD) [6, 7, 8]
    - Spatial reconstruction: 2nd-order TVD or 3rd-order WENO
    - Hyperbolic solver: Multidimensional Riemann solver [6]

Numerical Approach

- Fluid equations:
  - Spatial reconstruction: 2nd-order TVD
  - Hyperbolic solver: HLLC solver
  - Temporal discretization: explicit RK2
- Maxwell equations $\rightarrow$ divergence-free techniques:
  - **Finite-difference time-domain** (FDTD) [1, 2, 3]
    - **implicit Crank-Nicolson** [4, 5] $\rightarrow c$ constraint
  - **Finite-volume time-domain** (FVTD) [6, 7, 8]
    - Spatial reconstruction: 2nd-order TVD or 3rd-order WENO
    - Hyperbolic solver: Multidimensional Riemann solver [6]
    - Temporal discretization: explicit RK2 with **sub-cycling** $\rightarrow c$ constraint

Numerical Approach

- Fluid equations:
  - Spatial reconstruction: 2nd-order TVD
  - Hyperbolic solver: HLLC solver
  - Temporal discretization: explicit RK2
- Maxwell equations $\rightarrow$ divergence-free techniques:
  - **Finite-difference time-domain** (FDTD) [1, 2, 3]
    - **implicit Crank-Nicolson** [4, 5] $\rightarrow c$ constraint
  - **Finite-volume time-domain** (FVTD) [6, 7, 8]
    - Spatial reconstruction: 2nd-order TVD or 3rd-order WENO
    - Hyperbolic solver: Multidimensional Riemann solver [6]
    - Temporal discretization: explicit RK2 with **sub-cycling** $\rightarrow c$ constraint
- Source terms:

Numerical Approach

- Fluid equations:
  - Spatial reconstruction: 2nd-order TVD
  - Hyperbolic solver: HLLC solver
  - Temporal discretization: explicit RK2
- Maxwell equations $\rightarrow$ divergence-free techniques:
  - **Finite-difference time-domain** (FDTD) [1, 2, 3]
    - **implicit Crank-Nicolson** [4, 5] $\rightarrow c$ constraint
  - **Finite-volume time-domain** (FVTD) [6, 7, 8]
    - Spatial reconstruction: 2nd-order TVD or 3rd-order WENO
    - Hyperbolic solver: Multidimensional Riemann solver [6]
    - Temporal discretization: explicit RK2 with **sub-cycling** $\rightarrow c$ constraint
- Source terms:
  - Strang splitting

Numerical Approach

- Fluid equations:
  - Spatial reconstruction: 2nd-order TVD
  - Hyperbolic solver: HLLC solver
  - Temporal discretization: explicit RK2
- Maxwell equations $\rightarrow$ divergence-free techniques:
  - **Finite-difference time-domain** (FDTD) [1, 2, 3]
    - **implicit Crank-Nicolson** [4, 5] $\rightarrow$ c constraint
  - **Finite-volume time-domain** (FVTD) [6, 7, 8]
    - Spatial reconstruction: 2nd-order TVD or 3rd-order WENO
    - Hyperbolic solver: Multidimensional Riemann solver [6]
    - Temporal discretization: explicit RK2 with **sub-cycling** $\rightarrow$ c constraint
- Source terms:
  - Strang splitting
  - locally implicit midpoint method [9] $\rightarrow$ CFL constraint

Locally implicit source treatment [10, 9]

The conserved variables are grouped into three categories

$$\boldsymbol{U}_1 = \{\rho_i, \rho_e, \boldsymbol{B}\}^\intercal, \quad \boldsymbol{U}_2 = \{\rho_i \boldsymbol{v}_i, \rho_e \boldsymbol{v}_e, \boldsymbol{E}\}^\intercal, \quad \boldsymbol{U}_3 = \{\mathcal{E}_i, \mathcal{E}_e\}^\intercal$$

then the (first-order [10]) update formula can be written as:

$$\boldsymbol{U}_1^{n+1} = \overline{\boldsymbol{U}}_1^n \tag{0.8}$$

$$\boldsymbol{U}_2^{n+1} = \overline{\boldsymbol{U}}_2^n + \Delta t\, \boldsymbol{A}(\boldsymbol{U}_1^{n+1})\boldsymbol{U}_2^{n+1} \tag{0.9}$$

$$\boldsymbol{U}_3^{n+1} = \overline{\boldsymbol{U}}_3^n + \Delta t\, \boldsymbol{S}_3(\boldsymbol{U}_1^{n+1}, \boldsymbol{U}_2^{n+1}) \tag{0.10}$$

The implicit step can be written as:

$$\boldsymbol{U}_2^{n+1} = (\mathbb{I} - \Delta t\, \boldsymbol{A}(\boldsymbol{U}_1^{n+1}))^{-1}\overline{\boldsymbol{U}}_2^n \tag{0.11}$$

Remark

This update allows a high CFL number. Second-order accuracy achieved by using the implicit midpoint method [9]

Innovations

Innovations: FDTD (divergence-free technique)

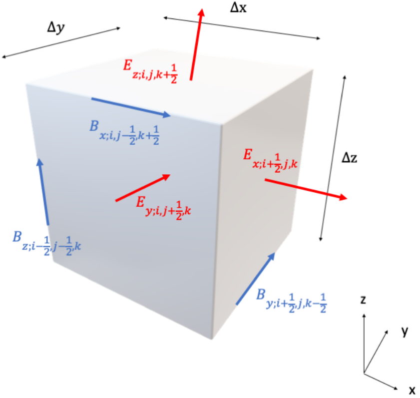

Figure: Collocation of the electromagnetic fields in FDTD. The magnetic field is defined at the edges and the electric field is defined at the faces.

Innovations: FDTD

It is based on a second-order accurate Crank-Nicolson scheme and the semi-implicit discretization can be written as

$$\frac{\boldsymbol{E}^{n+1} - \boldsymbol{E}^{n}}{\Delta t} = c^2 \left(\frac{1}{2} \nabla \times \boldsymbol{B}^{n} + \frac{1}{2} \nabla \times \boldsymbol{B}^{n+1} \right) \tag{0.12}$$

$$\frac{\boldsymbol{B}^{n+1} - \boldsymbol{B}^{n}}{\Delta t} = - \left(\frac{1}{2} \nabla \times \boldsymbol{E}^{n} + \frac{1}{2} \nabla \times \boldsymbol{E}^{n+1} \right) \tag{0.13}$$

which can be rearranged into the implicit equation

$$\left(1 - \frac{c^2 \Delta t^2}{4} \nabla^2 \right) \left[\frac{\boldsymbol{B}^{n+1} - \boldsymbol{B}^{n}}{\Delta t} \right] = -\nabla \times \boldsymbol{E}^{n} + \frac{c^2 \Delta t}{2} \nabla^2 \boldsymbol{B}^{n} \tag{0.14}$$

Remark

This implicit update relaxes the speed of light constraint.

Innovations: FVTD (divergence-free technique)

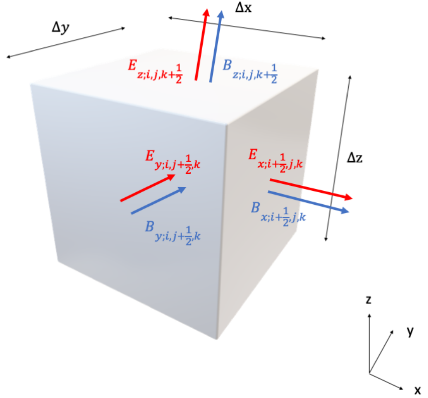

Figure: Collocation of the electromagnetic fields in FVTD. The magnetic field and the electric field are defined at the faces.

Innovations: FVTD

The explicit update for the x-components in 2D are

$$B^{n+1}_{x,i+\frac{1}{2},j} = B^{n}_{x,i+\frac{1}{2},j} - \frac{\Delta t}{\Delta y}\left(E^{*}_{z,i+\frac{1}{2},j+\frac{1}{2}} - E^{*}_{z,i+\frac{1}{2},j-\frac{1}{2}}\right) \tag{0.15}$$

$$E^{n+1}_{x,i+\frac{1}{2},j} = E^{n}_{x,i+\frac{1}{2},j} + c^2\frac{\Delta t}{\Delta y}\left(B^{*}_{z,i+\frac{1}{2},j+\frac{1}{2}} - B^{*}_{z,i+\frac{1}{2},j-\frac{1}{2}}\right) \tag{0.16}$$

where B^*_z and E^*_z are states from the Multidimensional Riemann solver [6].

Remark

These updates are constrained by the speed of light. Sub-cycling can be used to relax the constraint.

Innovations: Projection methods [11, 12]

Remark

Projection methods are used to reduce divergence errors from averaging electric fields from cell centers to cell faces.

One can express the electric field (with divergence errors) $\boldsymbol{E}^*$ in terms of a constraint-preserving part $\boldsymbol{E}^c$ and a scalar ϕ as

$$\boldsymbol{E}^* = \boldsymbol{E}^c + \nabla\phi \tag{0.17}$$

so that one can solve for the potential ϕ as

$$\nabla^2\phi = \nabla\cdot\boldsymbol{E}^* - \frac{\sigma}{\epsilon_0} \tag{0.18}$$

and the constraint-preserving electric field can be recovered as

$$\boldsymbol{E}^c = \boldsymbol{E}^* - \nabla\phi \tag{0.19}$$

Pointwise description

1. update the source terms at cell centers for $\Delta t_{fluid}/2$
2. obtain face-averaged electric field
3. advance the fluid variables for Δt_{fluid} using spatial reconstructions and RK time stepping
4. use FDTD with an implicit update for Δt_{fluid} or use FVTD with sub-cycling with Δt_c
5. obtain cell-averaged electromagnetic fields
6. update the source terms at cell centers for $\Delta t_{fluid}/2$
7. obtain face-averaged electric field
8. use projection methods to reduce electric divergence errors

Results

Results

- Computational Framework: AMReX

Results

- Computational Framework: AMReX
- Parallelization using MPI

Results

- Computational Framework: AMReX
- Parallelization using MPI
- Run on a desktop with 16 cores unless otherwise specified

Results

- Computational Framework: AMReX
- Parallelization using MPI
- Run on a desktop with 16 cores unless otherwise specified
- Aim will be to compare implicit FDTD and explicit FVTD with sub-cycling

Results

- Computational Framework: AMReX
- Parallelization using MPI
- Run on a desktop with 16 cores unless otherwise specified
- Aim will be to compare implicit FDTD and explicit FVTD with sub-cycling
- FVTD results used 2nd-order TVD unless otherwise specified

Results

- Computational Framework: AMReX
- Parallelization using MPI
- Run on a desktop with 16 cores unless otherwise specified
- Aim will be to compare implicit FDTD and explicit FVTD with sub-cycling
- FVTD results used 2nd-order TVD unless otherwise specified
- As a reference, results using HDC and FVTD without sub-cycling are also shown

Results: Brio and Wu Test

Computational domain: $[0, 1]$ Transmissive boundaries								
	ρ_i	ρ_e	$\boldsymbol{v}_\alpha$	p_α	B_x	B_y	B_x	$\boldsymbol{E}$
Left	1.0	$1.0/m$	$\mathbf{0.0}$	0.5	0.75	1.0	0.0	$\mathbf{0.0}$
Right	0.125	$0.125/m$	$\mathbf{0.0}$	0.05	0.75	-1.0	0.0	$\mathbf{0.0}$

Table: Initial data for the two-fluid Brio and Wu test.

$\gamma = 5/3$, $r_{L_i} = \{1, 0.1\}$, $\lambda_D = 0.01$, $m = m_i/m_e = 1836$ and $c = 100$

Results: Brio and Wu Test

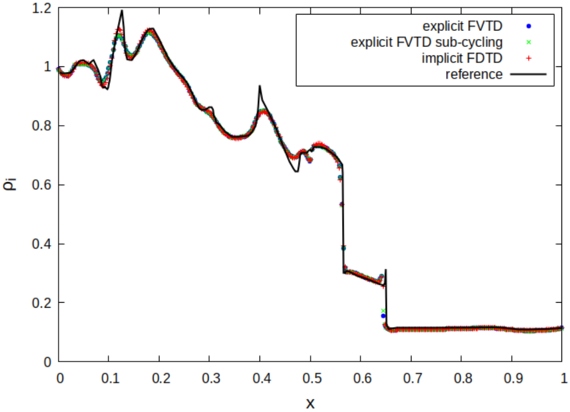

Figure: Ion density for the two-fluid Brio and Wu test for $r_{L_i} = 0.1$ using 1024 cells at $t = 0.1$. Reference from Abgrall and Kumar [10] using 10016 cells.

Results: Brio and Wu Test

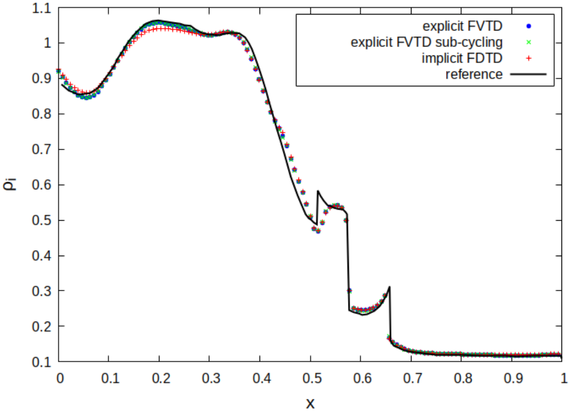

Figure: Ion density for the two-fluid Brio and Wu test for $r_{L_i} = 1$ using 1024 cells at $t = 0.1$. Reference from Abgrall and Kumar [10] using 10016 cells. FVTD solutions were slightly more accurate.

Results: Brio and Wu Test

Maxwell	Time stepping	Steps	CPU time (s)	CPU time/step (s)
FVTD	explicit	25600	250.46	$9.78 \cdot 10^{-3}$
FVTD	explicit sub-cycling	13115	147.51	$1.12 \cdot 10^{-2}$
FDTD	implicit	13281	174.14	$1.31 \cdot 10^{-2}$

Table: CPU timings for the Brio and Wu test for $r_{L_i} = 1$.

Observations

Sub-cycling and implicit time stepping reduced the number of steps and the CPU times. In this problem, $\Delta t_{fluid} \approx 2\Delta t_c$ and sub-cycling is more efficient.

Results: Ideal MHD Orszag-Tang Vortex

Computational domain: $[0, 2\pi] \times [0, 2\pi]$ Periodic boundaries				
ρ_α	$\boldsymbol{v}_\alpha$	p_α	$\boldsymbol{B}$	$\boldsymbol{E}$
γ^2	$\begin{pmatrix} -\sin(y) \\ \sin(x) \\ 0.0 \end{pmatrix}$	γ	$\begin{pmatrix} -\sin(y) \\ \sin(2x) \\ 0.0 \end{pmatrix}$	$-\boldsymbol{v}_\alpha \times \boldsymbol{B}$

Table: Initial data for the ideal MHD Orszag-Tang vortex.

$\gamma = 5/3$, $r_{L_i} = 0.01$, $\lambda_D = 0.1$, $r_i = -r_e = 1$ and $c = 10$

Remark

Small Larmor radius r_{L_i} models the MHD regime.

Results: Ideal MHD Orszag-Tang Vortex

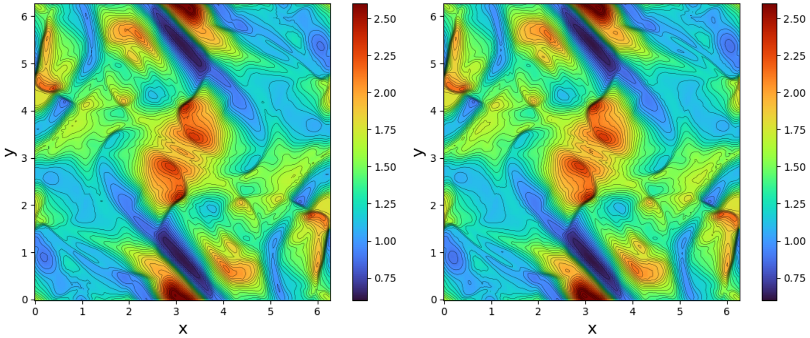

(a) Explicit HDC

(b) Explicit FVTD with sub-cycling

Figure: Ion density for the Orszag-Tang vortex using 256^2 cells at $t = 5$. Very similar solutions but HDC required some parameter tuning. HDC was also more expensive than FVTD.

Results: Ideal MHD Orszag-Tang Vortex

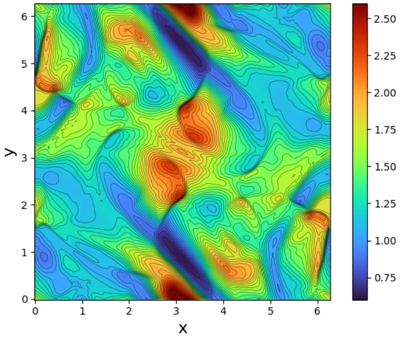

(a) Explicit HDC

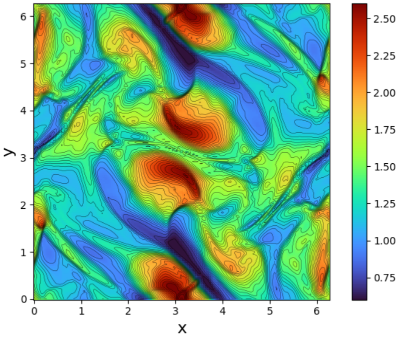

(b) Implicit FDTD

Figure: Ion density for the Orszag-Tang vortex using 256^2 cells at $t = 5$. FDTD captured better the features.

Results: Ideal MHD Orszag-Tang Vortex

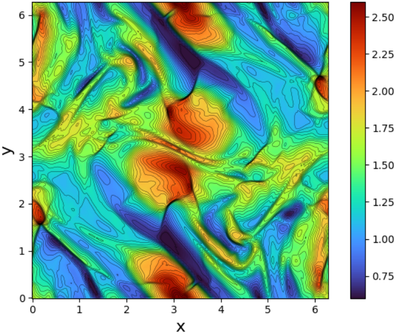

(a) Explicit HDC with 512^2 cells

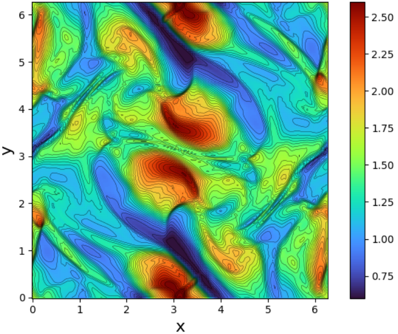

(b) Implicit FDTD with 256^2 cells

Figure: Ion density for the Orszag-Tang vortex at $t = 5$. FDTD solution was close to a high resolution solution.

Results: Ideal MHD Orszag-Tang Vortex

Maxwell	Time stepping	Steps	CPU time (s)	CPU time/step (s)
HDC	explicit	5093	911.64	0.18
FVTD	explicit sub-cycling	1147	235.41	0.21
FDTD	implicit	1205	203.84	0.17

Table: CPU timings for the ideal MHD Orszag-Tang vortex using 256^2 cells.

The high resolution (512^2 cells) fully explicit HDC method took $7514.98s$ (about 35 times more than the low resolution implicit FDTD method).

Observations

In this problem $\Delta t_{fluid} \approx 4\Delta t_c$. When the speed of light is much higher than the fluid speeds, sub-cycling loop becomes more expensive and less efficient than implicit time stepping.

Computational domain: $[-L_x/2, L_x/2] \times [-L_y/2, L_y/2]$ Periodic in the x-direction and conducting wall in the y-axis			
n	$v_{z,e}$	p	B_x
$n_0(sech^2(\frac{y}{\lambda}) + \frac{1}{5})$	$j_z/n_e q_e$	$B_0^2/2\,(sech^2(\frac{y}{\lambda}) + \frac{1}{5})$	$B_0 tanh(\frac{y}{\lambda})$

Table: Initial data for the unperturbed Harris sheet configuration.

Perturbation: $-\hat{\boldsymbol{e}}_z \times \nabla\left(\frac{1}{10}\cos\left(\frac{2\pi x}{L_x}\right)\cos\left(\frac{\pi y}{L_y}\right)\right)$

$n_0 = 1.0$, $B_0 = 1.0$ $\lambda = 0.5$, $L_x = 25.6$, $L_y = 12.8$

$\gamma = 5/3$, $r_{L_i} = 1$, $\lambda_D = 0.1$, $m_i/m_e = 25$ and $c = 10$

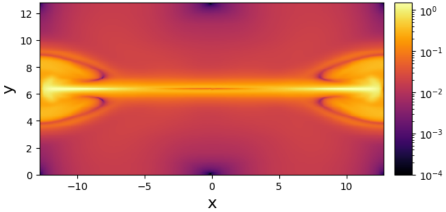

(a) Explicit FVTD with sub-cycling

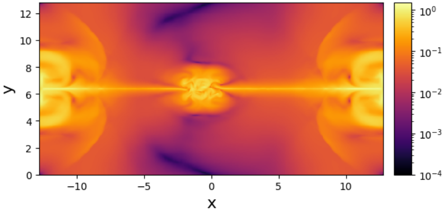

(b) Implicit FDTD

Figure: Ion momentum for the GEM reconnection challenge with using 512×256 cells at $t = 25$ (log-scale). The central magnetic island could be captured by the FDTD method.

Results: GEM Reconnection Challenge

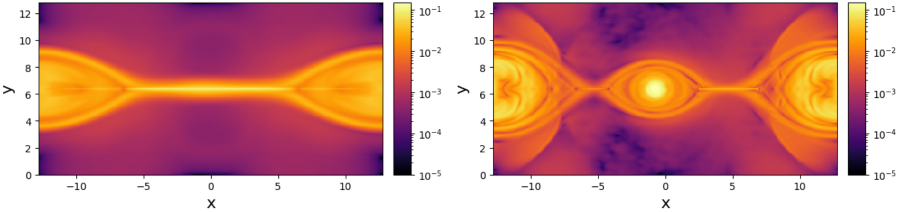

(a) Explicit FVTD with sub-cycling

(b) Implicit FDTD

Figure: Electron momentum for the GEM reconnection challenge with using 512×256 cells at $t = 25$ (log-scale). The central magnetic island could be captured by the FDTD method.

Results: GEM Reconnection Challenge

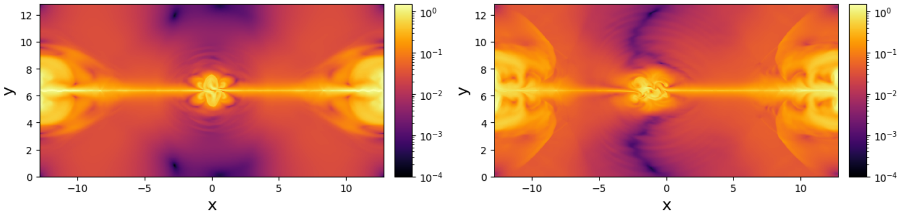

(a) Explicit FVTD with sub-cycling

(b) Implicit FDTD

Figure: Ion momentum for the GEM reconnection challenge using 1024×512 cells at $t = 25$ (log-scale). FVTD method needed high resolution to capture the magnetic island.

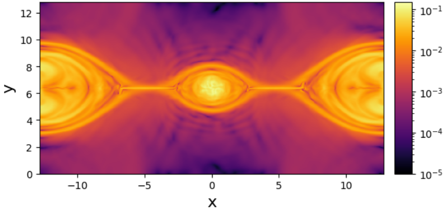

(a) Explicit FVTD with sub-cycling

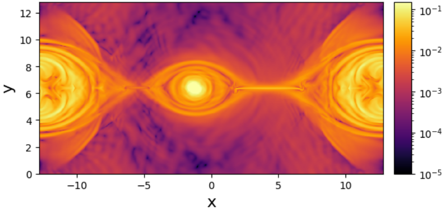

(b) Implicit FDTD

Figure: Electron momentum for the GEM reconnection challenge using 1024×512 cells at $t = 25$ (log-scale). FVTD method needed high resolution to capture the magnetic island.

Results: GEM Reconnection Challenge

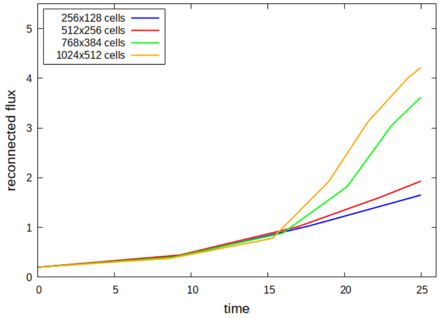

(a) Explicit FVTD with sub-cycling

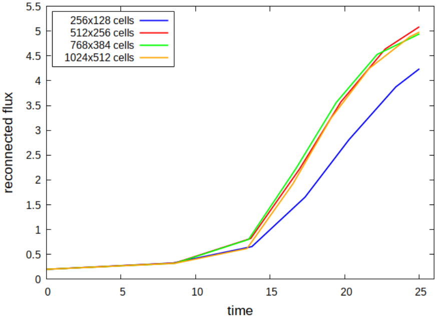

(b) Implicit FDTD

Figure: Reconnected fluxes for the GEM reconnection challenge. The FDTD method reached convergence faster.

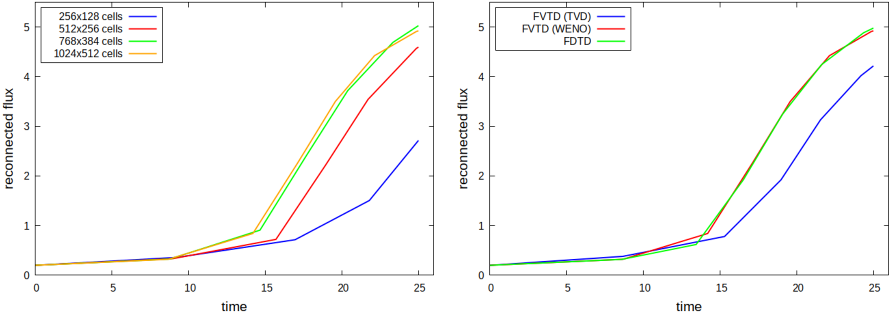

(a) FVTD (WENO) with sub-cycling

(b) Comparison using 1024×512 cells

Figure: Reconnected fluxes for the GEM reconnection challenge. FVTD with 3rd-order WENO is also shown (all previous FVTD results used 2nd-order TVD). FVTD with WENO and FDTD solutions had the same reconnected fluxes.

Results: GEM Reconnection Challenge

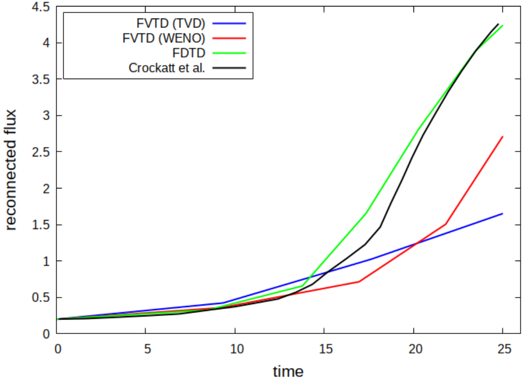

Figure: Reconnected fluxes for the GEM reconnection challenge using 256×128 cells. Reference solutions from Crockatt et al. [13] using 960×480 cells. The low resolution implicit FDTD method produced a similar reconnected flux to the high resolution reference case.

Conclusion

Concluding remarks

- The speed of light constraint was relaxed and divergence-free methods were used

Concluding remarks

- The speed of light constraint was relaxed and divergence-free methods were used
- Implicit FDTD method was more efficient in most problems

Concluding remarks

- The speed of light constraint was relaxed and divergence-free methods were used
- Implicit FDTD method was more efficient in most problems
- FVTD method was better for problems with very strong initial discontinuities (e.g. Brio and Wu test)

Concluding remarks

- The speed of light constraint was relaxed and divergence-free methods were used
- Implicit FDTD method was more efficient in most problems
- FVTD method was better for problems with very strong initial discontinuities (e.g. Brio and Wu test)
- FVTD method with 3rd-order WENO

Concluding remarks

- The speed of light constraint was relaxed and divergence-free methods were used
- Implicit FDTD method was more efficient in most problems
- FVTD method was better for problems with very strong initial discontinuities (e.g. Brio and Wu test)
- FVTD method with 3rd-order WENO
  - More efficient (at achieving given accuracy) than FVTD with 2nd-order TVD

Concluding remarks

- The speed of light constraint was relaxed and divergence-free methods were used
- Implicit FDTD method was more efficient in most problems
- FVTD method was better for problems with very strong initial discontinuities (e.g. Brio and Wu test)
- FVTD method with 3rd-order WENO
  - More efficient (at achieving given accuracy) than FVTD with 2nd-order TVD
  - More expensive than FDTD method

Concluding remarks

- The speed of light constraint was relaxed and divergence-free methods were used
- Implicit FDTD method was more efficient in most problems
- FVTD method was better for problems with very strong initial discontinuities (e.g. Brio and Wu test)
- FVTD method with 3rd-order WENO
  - More efficient (at achieving given accuracy) than FVTD with 2nd-order TVD
  - More expensive than FDTD method
  - Higher-order WENO might become more efficient

Concluding remarks

- The speed of light constraint was relaxed and divergence-free methods were used
- Implicit FDTD method was more efficient in most problems
- FVTD method was better for problems with very strong initial discontinuities (e.g. Brio and Wu test)
- FVTD method with 3rd-order WENO
    - More efficient (at achieving given accuracy) than FVTD with 2nd-order TVD
    - More expensive than FDTD method
    - Higher-order WENO might become more efficient
- Next steps: 10-moment two-fluid model (and higher moments)

Concluding remarks

- The speed of light constraint was relaxed and divergence-free methods were used
- Implicit FDTD method was more efficient in most problems
- FVTD method was better for problems with very strong initial discontinuities (e.g. Brio and Wu test)
- FVTD method with 3rd-order WENO
  - More efficient (at achieving given accuracy) than FVTD with 2nd-order TVD
  - More expensive than FDTD method
  - Higher-order WENO might become more efficient
- Next steps: 10-moment two-fluid model (and higher moments)
  - 5-moment model assumes local thermal equilibrium

Concluding remarks

- The speed of light constraint was relaxed and divergence-free methods were used
- Implicit FDTD method was more efficient in most problems
- FVTD method was better for problems with very strong initial discontinuities (e.g. Brio and Wu test)
- FVTD method with 3rd-order WENO
    - More efficient (at achieving given accuracy) than FVTD with 2nd-order TVD
    - More expensive than FDTD method
    - Higher-order WENO might become more efficient
- Next steps: 10-moment two-fluid model (and higher moments)
    - 5-moment model assumes local thermal equilibrium
    - Higher-moment models describe the deviation from the local thermal equilibrium $\rightarrow$ transition from high to low collisionality plasmas

Acknowledgments

Special thanks to S.T. Millmore and N. Nikiforakis for invaluable guidance and mentorship. Appreciation to the Laboratory for Scientific Computing team members who contributed to various aspects of this work.

This work was supported by the University of Cambridge Harding Distinguished Postgraduate Scholars Programme and the Centre for Scientific Computing.

Thank you!

References I

[1] K. Yee. "Numerical solution of initial boundary value problems involving Maxwell's equations in isotropic media". In: *IEEE Transactions on antennas and propagation* 14.3 (1966), pp. 302–307.

[2] A. Taflove and M. E. Brodwin. "Numerical solution of steady-state electromagnetic scattering problems using the time-dependent Maxwell's equations". In: *IEEE transactions on microwave theory and techniques* 23.8 (1975), pp. 623–630.

[3] A. Taflove. "Review of the formulation and applications of the finite-difference time-domain method for numerical modeling of electromagnetic wave interactions with arbitrary structures". In: *Wave Motion* 10.6 (1988), pp. 547–582.

[4] C Sun and C. Trueman. "Unconditionally stable Crank-Nicolson scheme for solving two-dimensional Maxwell's equations". In: *Electronics letters* 39.7 (2003), pp. 595–597.

References II

[5] Y Yang, R. Chen, and E. K. Yung. "The unconditionally stable Crank Nicolson FDTD method for three-dimensional Maxwell's equations". In: *Microwave and Optical Technology Letters* 48.8 (2006), pp. 1619–1622.

[6] D. S. Balsara et al. "A high-order relativistic two-fluid electrodynamic scheme with consistent reconstruction of electromagnetic fields and a multidimensional Riemann solver for electromagnetism". In: *Journal of Computational Physics* 318 (2016), pp. 169–200.

[7] D. S. Balsara et al. "Computational electrodynamics in material media with constraint-preservation, multidimensional Riemann solvers and sub-cell resolution–Part I, second-order FVTD schemes". In: *Journal of Computational Physics* 349.C (2017).

[8] D. S. Balsara et al. "Computational electrodynamics in material media with constraint-preservation, multidimensional Riemann solvers and sub-cell resolution–Part II, higher order FVTD schemes". In: *Journal of Computational Physics* 354 (2018), pp. 613–645.

References III

[9] L. Wang et al. "Exact and locally implicit source term solvers for multifluid-Maxwell systems". In: *Journal of Computational Physics* 415 (2020), p. 109510.

[10] R. Abgrall and H. Kumar. "Robust finite volume schemes for two-fluid plasma equations". In: *Journal of Scientific Computing* 60 (2014), pp. 584–611.

[11] J. Bell, L. Howell, and P. Colella. "An efficient second-order projection method for viscous incompressible flow". In: *10th Computational Fluid Dynamics Conference*. 1991, p. 1560.

[12] J. U. Brackbill and D. C. Barnes. "The effect of nonzero $\nabla \cdot \boldsymbol{B}$ on the numerical solution of the magnetohydrodynamic equations". In: *Journal of Computational Physics* 35.3 (1980), pp. 426–430.

[13] M. M. Crockatt et al. "An implicit monolithic AFC stabilization method for the CG finite element discretization of the fully-ionized ideal multifluid electromagnetic plasma system". In: *Journal of Computational Physics* 464 (2022), p. 111228.